Analysis of multi-scale radiometric data collected during the Cold Land Processes Experiment -1 (CLPX-1)

M. Tedesco[1], E.J. Kim[2], A. Gasiewski[3] and B. Stankov[3]

Brightness temperature maps at 18.7 and 37 GHz collected at the Fraser and North Park Meso-Scale Areas during the Cold Land Processes Experiment by the NOAA Polarimetric Scanning Radiometer (PSR/A) airborne sensor are analyzed. The Fraser site is mostly covered by forest with a typical snowpack depth of 1 m while North Park has no forest cover and is characterized by patches of shallow snow. We examine histograms of the brightness temperatures at 500 m resolution for both the Fraser and North Park areas. The histograms can be modelled by a log-normal distribution in the case of the Fraser MSA and by a bi-modal distribution in the case of the North Park MSA. The histograms of the brightness temperatures at coarser resolutions are also plotted to study the effects of sensor resolution on the shape of the distribution, on the values of the average brightness temperatures and standard deviations. Finally, the values of brightness temperatures obtained by re-sampling (aggregating) the data at 25 km resolution are compared with the values of the brightness temperatures collected by the Advanced Microwave Scanning Radiometer (AMSR-E) and Special Sensor Microwave/Imager (SSM/I) satellite radiometers. The results show that in both areas for sensor footprint larger than 5000 m, the brightness temperatures show a flat distribution and the memory of the initial distribution is lost. The values of the brightness temperatures measured by the satellite radiometers are in good agreement with the values obtained averaging the airborne data, even if some discrepancies occur.

[1] Goddard Earth Science Technology Center - UMBC, NASA Goddard Space Flight Center, USA

[2] Laboratory Of Hydrospheric and Biospheric Processes, NASA Goddard Space Flight Center, USA

[3]ETL – NOAA, USA

mail to: mtedesco@umbc.edu; marco.tedesco@gsfc.nasa.gov

1. Introduction

Snow represents a fundamental component of the Earth's water cycle, covering more than the half of the Northern hemisphere land surface (around 60 %) in mid winter. Over 30% of Earth's total land surface is covered by seasonal snow [Robinson, et al., 1993]. Microwaves are sensitive to snow parameters [i.e. Macelloni et al., 2001; Tedesco, 2003], which can be estimated using algorithms based on passive microwave remote sensing observations [i.e. Hallikainen and Jolma, 1992; Foster et al. 1997; Tait, 1998; Kelly et al., 2003; Tedesco et al., 2004]. At microwave frequencies, neither solar illumination nor clouds limit the retrieval of snow parameters, permitting frequent and consistent observations. Accurate estimates of snow water equivalent and other parameters play an important role in weather and climate models, in natural hazard forecasting, and in water resources applications. The retrieval of such parameters from microwave remotely-sensed data has many advantages, but a discrepancy exists between the small scale at which many snow parameters are measured and understood and the large-scale footprints of current microwave satellite sensors (25x25 km2). At large scales, the heterogeneity of the terrain within the pixel is a limiting factor for the use of forward radiative transfer models to reproduce the observed brightness temperatures using point scale or area-aggregated snow properties. In this paper, we use microwave data collected during the Cold Land Processes Experiment-1 (CLPX-1) to study these limitations and to improve the understanding of scaling-related issues. One of the principal tasks of CLPX-1 was to understand at what scale the spatial variability of snow characteristics control fluxes, the transformation of water and energy and if remote sensing can resolve the variability at these scales (http://www.nohrsc.nws.gov/~cline/clpx.html). Within this framework, intensive ground, airborne and space-borne data were collected in several study areas in Colorado, central Rocky Mountain of the western United States, during February and March of 2002 and 2003.

In this study, we analyze the brightness temperatures at 18.7 and 37 GHz acquired by an airborne passive microwave imager NOAA Polarimetric Scanning Radiometer (PSR/A) and by the Advanced Microwave Scanning Radiometer (AMSR-E) and Special Sensor Microwave/Imager (SSM/I) satellite radiometers during the third Intensive Observation Period (IOP3, dry snow, February 19 - 25, 2003). In particular, we concentrate on the data collected over the Fraser and North Park Meso-Scale Areas (MSAs, http://www.nohrsc.nws.gov/~cline/clpx.html). The brightness temperatures collected by the airborne and space-borne instruments are re-sampled, respectively, at 500 m (PSR/A) and 25 km (SSM/I and AMSR-E) resolutions. The effect of sub-pixel heterogeneity (e.g., the presence of forest inside the pixel) and the varying

overflight times are considered as possible causes of the observed differences. Histograms of the brightness temperatures collected by the PSR/A over the Fraser and North Park MSAs are plotted at different resolutions, from 500 m to 25 Km. Histograms at 500m resolution are used to identify distribution functions for both MSAs. The effect of a coarser resolution on the shape of the distribution is studied as well as its effect on the average values of the brightness temperatures. At 25 km resolution, microwave brightnesses are also compared with those from the SSM/I and AMSR-E satellite radiometers.

The paper is organized as follows: in the first Section the location of the MSAs is reported and the characteristics of the CLPX-1 areas are described. In the second Section we briefly describe the instruments used to collect the brightness temperatures and we show an example of the data collected by the PSR/A. The third Section discusses the analysis of the brightness temperatures at different scales. Finally, in the last Section, we report our conclusions.

2. Location and characteristics CLPX areas

Figure 1 shows a schematic diagram of the study areas for the CLPX-1 together with a map showing the locations of the selected areas. The largest study area is the large regional study area (LRSA, 375x375 Km^2) and it is located in northern Colorado and southern Wyoming, U.S.A. The small regional study area (SRSA) is located in north-central Colorado (105°-107.5° W, 39.5E-41E N), and it is approximately 215-km x 170-km. Nested within the SRSA there are three Meso-cell Study Areas (MSAs, 25-km x 25-km), used for airborne data collection. In this study, we concentrate on the brightness temperatures acquired at the Fraser and North Park MSAs. The Fraser MSA is a topographically complex area with a mean elevation of 3066 m (with a range of nearly 1400 m and a maximum elevation of 3962 m). The highest-elevation areas in the South are predominantly alpine tundra or bare rock. The mountain areas are dominated by dense coniferous forests. The North Park MSA has a mean elevation of 2499 m. Most of the vegetation is sage-grassland, with willow along riparian areas. Snowpacks in this area tend to be shallow, and are typical of prairie and arctic- and alpine- tundra snow covers.

3. The radiometric acquisition systems and data

Brightness temperatures at fine resolution (~ 100 m, depending on topography) were collected by means of the NOAA Polarimetric Scanning Radiometer, an airborne multi-band conical-scanned imaging radiometer system [e.g., Piepmeier and Gasiewski, 1996]. PSR/A includes a single scanhead that provides imagery at most of the AMSR-E imaging bands, with an observation angle of 53° with respect to nadir. As an example of the collected data, Figure 2 shows the brightness temperatures at 37 GHz, vertical polarization, collected on February 23, 2003 at the Fraser (a), North Park (b) MSAs. The exact size of the antenna footprint is mainly a function of the terrain elevation as the aircraft altitude above sea level was almost constant during the flights. At high frequencies (37 and 89 GHz), the size of the antenna footprint ranges between 84 and 350 meters while at 18.7 GHz it ranges between 229 and 749 meters. As the PSR/A is a conical-scanned radiometer, the shape of the footprint on the ground depends on the relative orientation of the scene to the 53° half-cone angle. However, the data collected by the PSR/A used in this study were re-sampled to obtain square pixels with a resolution of 500 m, at all frequencies. This value is selected because it is the minimum value which guarantees complete coverage of the observed areas using a square pixel.

Calibrated and geo-located satellite brightness temperatures, acquired over the LRSA using the SSM/I and AMSR-E radiometers were obtained from the National Snow and Ice Data Center (NSIDC) [Brodzik 2003a, 2003b]. We consider both ascending and descending orbit data, in order to assure the highest number of available observations.

4. Results and discussion

Figure 3 shows the histograms of the brightness temperatures collected by the PSR/A over the Fraser and North Park MSAs (500 m res.) on February 23, 2003 at 18.7 and 37 GHz (vertical polarization). The values of the brightness temperatures observed by the SSM/I and AMSR-E radiometers are also depicted with arrows (continuous lines for AMSR-E and dotted for SSM/I). Upward arrows indicate satellite observations during ascending orbits while downward arrows indicate observations during descending orbits. More in detail,

Figure 3 depicts the data collected at the Fraser MSA at (a) 18.7 and (b) 37 GHz and the data collected at the North Park MSA, also at (c) 18.7 and (d) 37 GHz.

The histograms of the brightnesses collected at the Fraser MSA show a single peak for high values of the brightness temperature, at both 18.7 and 37 GHz. The distribution of the brightness temperatures can be modeled using a log-normal distribution, negatively skewed. When radiometric data were acquired, the Fraser MSA was covered by snow with an average snow depth around 1 m and maxima around 2 meters. The effect of the trees on the histograms is mostly responsible for the shape of the histograms. A map of the forest cover fraction derived from 250 m resolution Normalized Difference Vegetation Index (NDVI) MODIS and 30 m resolution United States Geological Survey (USGS) Land Use Land Cover (LULC) maps is used to compute the forest cover fraction for each pixel at different resolutions [Tedesco et al. 2004]. A comparative analysis between the brightness temperatures and the forest cover fraction was carried out. The results show that brightness temperatures correspond to the highest values of the forest density. At 18.7 GHz the tail of the distribution is not as long as that of the 37 GHz. This can be explained considering that, in general, the values of brightness temperature at 18.7 GHz are influenced by the soil

underlying the snowpack and are higher than those at 37 GHz, which are more sensitive to the attenuating influence of the snowpack (lower brightness temperatures).

The distribution of the brightness temperatures collected at the North Park MSA, on the other hand, can be modeled using a bi-modal distribution. At the time of the data acquisition, the MSA was partially covered by snow (with average snow depth around 20 cm and a maximum snow depth around 45 cm). The areas with snow are responsible for the low values of brightness temperature and the snow-free areas are responsible for high values of brightness temperatures. This is confirmed by comparing the brightness temperatures collected by the PSR/A using snow covered area derived from MODIS. As it happened for the data collected at the Fraser MSA, the 37 GHz brightness temperatures appear to be noisier than those collected at 18.7 GHz.

Although space limitations prevents from showing the additional data, the results reported here for the vertical polarization can be extended to the horizontal polarization case for both Fraser and North Park MSAs, at all frequencies.

We next re-sample the PSR/A data at successively coarser resolutions and plot the corresponding histograms. The goal of this exercise is to understand at what spatial scale the histograms can still be described by the initial distribution. We consider five different resolutions for our analysis: 1000, 2500, 5000, 12500 and 25000 m. In the case of the Fraser MSA, the values of the peaks, the average values and standard deviations are reported in Table 1. As stated earlier, at 500 m resolution the histograms of the brightness temperatures can be modeled using a log-normal distribution, negatively skewed ($R^2 = 0.92$). Our analysis points out that this is still possible at a resolution of 1000 m ($R^2 = 0.76$). However, at a resolution of 2500 meters, two values of brightness temperatures at 37 GHz show the same number of occurrences, instead of a single peak. As the resolution gets coarser, the histograms become increasingly flat, the standard deviation decreases and the brightness temperatures concentrate around a value close to the average. This happens when the resolution reaches approximately 5000 m. In the case of the North Park MSA, the histograms of the brightness temperatures at 500 m resolution can be modeled using a bi-

modal distribution ($R^2 = 0.91$). This is still true at 1000 m resolution ($R^2 = 0.65$). At 2500 resolution, two peaks are still observable with the remaining brightness temperatures showing the same number of occurrences. However, the peak is made of two distinct values, which are very close at 18.7 GHz but they differ by about 10 K at 37 GHz. Also in this case, for the resolutions coarser than 5000 m, the histograms are flat.

We compare the values of brightness temperatures obtained re-sampling the PSR-A data at 25 km resolution with those recorded by the SSM/I and AMSR-E. In general, the values recorded by the space-borne instruments are consistent with those obtained averaging the PSR/A data. The observed differences between airborne and satellite data can be due to the atmospheric correction to be applied to the two data sets, to the terrain topography and to the time at which the data were acquired. The PSR/A flew on the areas at 20:30 UTC time. The AMSR-E passed at 19:54 UTC time (ascending orbit) and 8:49 UTC (descending orbit). The SSM/I passed at 14:18 UTC time (descending orbit). No coverage was available for the SSM/I with ascending orbit. In the case of the Fraser MSA, we observe that the brightness temperatures recorded by AMSR-E and SSM/I differ at maximum by 3.5 K from those obtained by averaging the PSR/A data to 25 km resolution, except for the observation from the SSM/I descending overpass at 37 GHz, which are 7.7 K lower than those of the PSR/A. This could be due to the fact that the SSM/I descending overflight occurred at night, when temperatures were cooler. Also in the case of the North Park MSA, the brightness temperatures recorded by the AMSR-E and SSM/I are consistent with those obtained by averaging the PSR/A data. In this case, best match is obtained in the case of the SSM/I descending overflight and the maximum error is obtained in the case of the AMSR-E ascending overflight at 37 GHz. The differences observed between the averaged PSR/A brightness temperatures and space-borne radiometric data can be due to the size of the antenna footprint of the AMSR-E and SSM/I, the position of the center of the antenna footprint and different calibration/validation procedures. In general, the same trend is observed considering the brightness temperatures at horizontal polarization.

5. Conclusions

The brightness temperatures collected using the high-resolution airborne NOAA Polarimetric Scanning Radiometer during the Cold Land Processes experiment-1 have been aggregated to simulate coarser resolutions. Histograms of the PSR/A brightness temperatures at finest resolution (500 m) display a log-normal distribution in the case of the Fraser forested area and a bi-modal distribution in the case of the patchy-snow not-forested North Park area. The histograms of the brightness temperatures at successively coarser resolutions have been studied to understand the effect of the pixel size on the shape of the distribution. For all examined cases, a threshold value of 5000 m resolution has been found after which the histograms of the brightness temperatures become flat (all brightness temperatures have the same number of occurrences). The values of the brightness temperatures obtained aggregating the PSR/A data to a 25 km resolution have been compared with the values of the brightness temperatures collected by the AMSR-E and SSM/I radiometers and were found to be within 7.7 K in the case of the Fraser area and 7.1 K in the case of the North Park area. In future studies, we will use the data collected during the Cold Land Processes Experiment during March 2002 and 2003 in order to extend the study to wet snow conditions.

6. Acknowledgement

We would like to thank Richard Armstrong and Mary Brodzik from the National Snow and Ice Data Center, Boulder, CO, for providing the SSM/I and AMSR-E brightness temperatures. We also would like to thank Dr. Richard Kelly for the constructive discussions and valuable assistance provided during the study.

References

[1] Foster, J. A. Chang, and D. Hall. (1997). Comparison of snow mass estimates from a prototype passive microwave snow algorithm, a revised algorithm and a snow depth climatology. *Remote Sensing of Environment. 62*: 132-142

[2] Hallikainen M. and Jolma P. (1992). Comparison of algorithms for the retrieval of snow water equivalent from NIMBUS-7 SMMR data in Finland. *IEEE Transactions on Geoscience and Remote Sensing, 30*, 124-131

[3] Kelly R. E., Chang A.T., Tsang L. and Foster J. (2003). A prototype AMSR-E global snow area and snow depth algorithm, IEEE Transactions on Geoscience and Remote Sensing, Vol. 41, No. 2

[4] G.Macelloni, S. Paloscia, P. Pampaloni and M. Tedesco. (2001). Microwave Emission from Dry Snow: A Comparison of Experimental and Model Result. *IEEE Trans. Geosci. Remote Sensing*, vol. 39, n. 12, pp. 2649-2656.

[5] Piepmeier J.R and Gasiewski A.J. (1996). Polarimetric scanning radiometer for airborne microwave imaging studies, *Proceedings of the International Geoscience and Remote Sensing Symposium, IGARSS'96, 2,* 1120 - 1122

[6] Robinson, D., Dewey, K., and R. Heim. (1993). Global snow cover monitoring: An update, *Bull. American Meteorological Society* 74, 1689-1696.

[7] Tait, A.(1998). Estimation of snow water equivalent using passive microwave radiation data. *Remote Sensing of Environment, 64*, 286-291.

[8] Tedesco M., J. Pulliainen, P. Pampaloni and M. Hallikainen (2004) ,Artificial neural network based techniques for the retrieval of SWE and snow depth from SSM/I data, *Remote Sensing of Environment*, Vol. 90/1, pp 76-85

[9] Tedesco M. (2003). *Microwave remote sensing of snow*, PhD Thesis, Institute of Applied Physics 'Carrara', Italian National Research Council, IFAC – CNR, Microwave Remote Sensing Group, November 2003

[10] Tedesco M., E. J. Kim, D. Cline, T. Graf, T. Koike, R. Armstrong, M. Brodzik, B. Stankov, A. Gasiewski and M. Klein (2004). Exploring scaling issues by using NASA Cold Land Processes Experiment (CLPX-1, IOP3) radiometric data, Proc. Of IGARSS 2004, Anchorage, AK

Figures and Tables

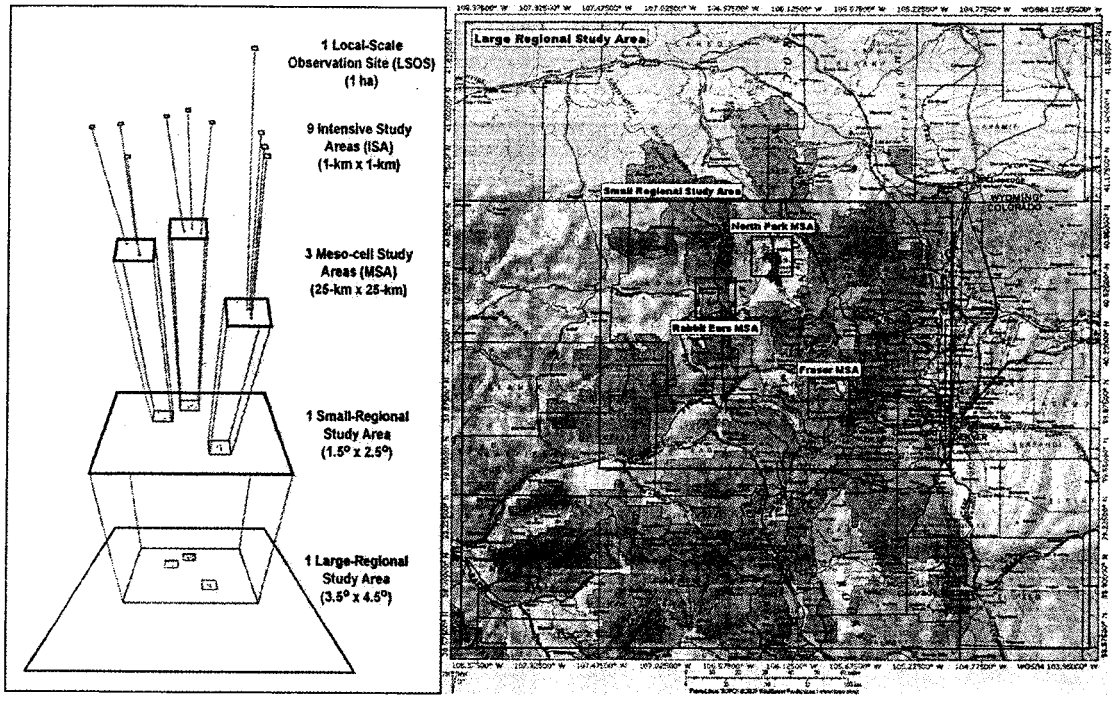

Figure 1 Schematic diagram and locations of the study areas for the CLPX-1

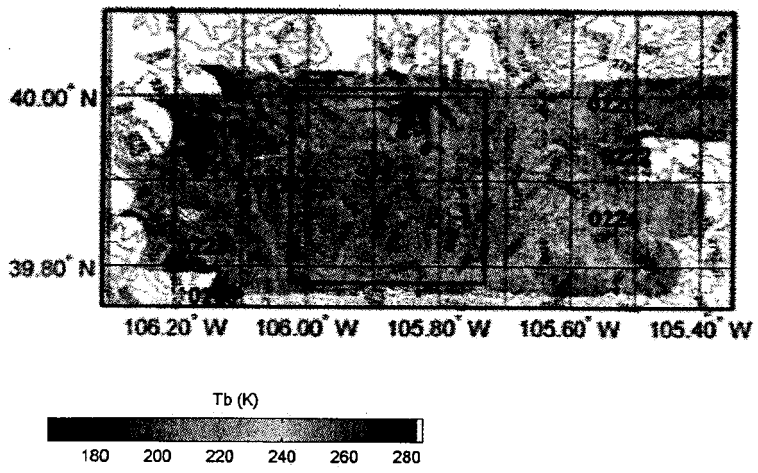

(a)

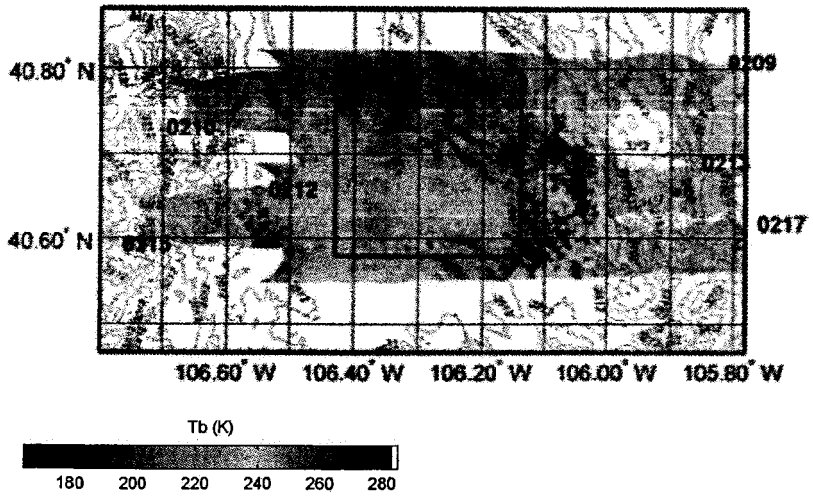

(b)

Figure 2 PSR image for 37 GHz channel vertical polarization on 23 February 2003 at Fraser (a) and North Park (b) Meso-Scale Areas. Numbers in the images represent the id acquisition number for PSR/A.

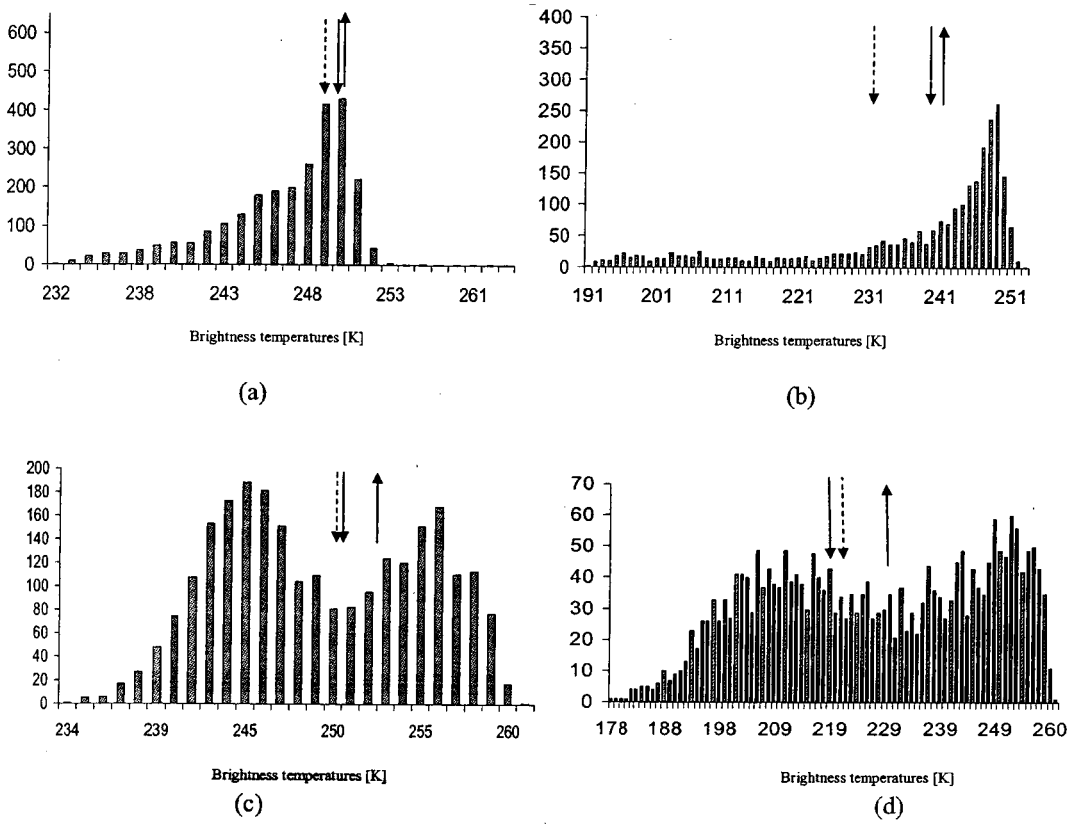

Figure 3 Histograms of PSR/A brightness temperatures at 19 GHz (left) and 37 GHz (right) for the Fraser (a,b) and North Park (c,d) MSAs. The brightness temperatures observed by the AMSR-E (solid arrow) and SSM/I (dotted arrow) are also reported. Upward arrows indicate satellite observations during ascending orbits while downward arrows indicate observations during descending orbits.

	18.7 GHZ			37 GHZ		
Res. [m]	*Weighted Avg. [K]*	*Peak Value [K]*	*Std. dev. [K]*	*Weighted Avg.[K]*	*Peak Value [K]*	*Std. dev. [K]*
500	249.3	250	6.2	240.1	249	21.9
1000	249.3	252.1	5.1	240.1	248.2	17.5
2500	249.3	250.1	4.7	240.1	245/249	11
5000	249.3	250.3	2.7	240.1	245.6	8.1
12500	249.3	n.a.	1.9	240.1	n.a.	3.1
25000	249.3	n.a.	n.a.	240.1	n.a.	n.a.
	Amsr-e Desc. [K]	*Amsr-e Asc. [K]*	*SSM/I Desc. [K]*	*Amsr-e Desc. [K]*	*Amsr-e Asc. [K]*	*SSM/I Desc. [K]*
	250.6	252.8	249.5	240.4	242.6	232.2

Table 1 Average values, peak values and standard deviations for the brightness temperatures collected at the Fraser MSA at different resolutions. The values of brightness temperatures observed from AMSR-E and SSM/I satellite radiometers are also reported.

	18.7 GHZ			37 GHZ		
Res. [m]	*Weighted Avg. [K]*	*Peak ValueS 1 and 2 [K]*	*Std. dev. [K]*	*Weighted Avg. [K]*	*Peak Values 1 and 2 [K]*	*Std.dev. [K]*
500	250.7	249, 258.7	7.9	224.7	208, 250.2	25
1000	250.7	245.1,258.3	7	224.7	210.2,245.7	25.5
2500	250.7	247, 257/259	7.7	224.7	205.1, 240/250	18.5
5000	250.7	n.a., 258.4	8.34	224.7	n.a., n.a.	16.9
12500	250.7	n.a., n.a	9	224.7	n.a., n.a	18.8
25000	250.7	n.a, n.a.	n.a.	224.7	n.a, n.a.	n.a.
	Amsr-e Desc. [K]	*Amsr-e Asc. [K]*	*SSM/I Desc. [K]*	*Amsr-e Desc. [K]*	*Amsr-e Asc. [K]*	*SSM/I Desc. [K]*
	249.5	253.2	249.2	219.4	230.2	223.9

Table 2 Average values, peak values and standard deviations for the brightness temperatures collected at the Fraser MSA at different resolutions. The values of brightness temperatures observed from AMSR-E and SSM/I satellite radiometers are also reported.